On the Trade-off Between Positioning and Data Rate for mm-Wave Communication

Giuseppe Destino* and Henk Wymeersch†

*University of Oulu, Oulu, Finland

†Chalmers University of Technology, Gothenburg, Sweden

email: giuseppe.destino@oulu.fi, henkw@chalmers.se

***Abstract*—millimeter wave (mmW) communication systems have the potential to increase data rates with low-latency, highly directional communication links. Due to the geometric nature of the propagation, mmW signals can also be used for accurate positioning. This paper explores the trade-off between communication rate and positioning quality in mmW systems. We show how rate and positioning quality interact as a function of bandwidth, number of antennas, and receiver location.**

I. Introduction

The next generation of wireless communication systems (so-called 5G), will be characterized by a move towards new frequency bands and the use of massive antenna arrays. In particular, the mmW spectrum (30–300 GHz) leads to "quasi-optical" propagation characteristics of radio signals [1]. The increased path loss at these frequencies can be counter-acted by employing highly directional transmit and receive beamforming to achieve sufficient signal-to-noise ratio (SNR) gain for high data rate communication. A challenge in beamforming is the initial beam-alignment that needs to be completed, prior to communication. To address this, fast beam alignment procedures have been devised [2], [3]. The final achievable data rate depends on the quality of the beam alignment procedure, where a fast sub-optimal procedure generally leads to worse alignment and lower throughput. These methods can provide a complexity that is sub-linear in the codebook size.

In addition to providing high-rate communication, mmW technology is also a key enabler for accurate positioning [4]–[6]. In contrast to conventional positioning, mmW beamforming allows (i) the determination of a user's position from a single access point, and (ii) the determination of the orientation of the user, with respect to the access point. Positioning is based on processing training signals from different beams and can thus be accomplished during the beam-alignment process.

Clearly, a longer beam alignment with more beams leads to more information for positioning, and thus better positioning quality. It is thus clear that there is a natural connection between throughput and positioning quality. This connection was previously investigated in [7]–[9], where [7] considered power optimization under rate and positioning constraint, while in [8] and [9], position information was harnessed to speed up beam alignment.

In this paper, we explore the trade-off between communication rate and positioning quality for single user LOS mmW communication, assuming a finite coherence time. We quantify the rate as a function of the codebook size and derive lower bounds on the achievable positioning quality. Combined, they allow us to visualize their trade-off, which can be used in the design of 5G joint communication and positioning systems.

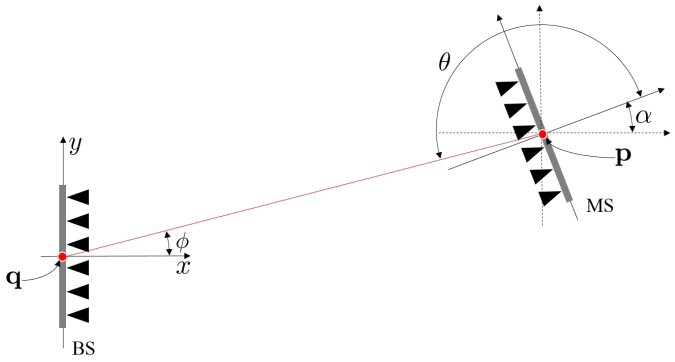

Figure 1. Geometry of the communication system including a transmitter with fixed location and orientation, and a receiver with unknown location $\mathbf{p}$ and orientation α.

II. mmW single-user MIMO system

A. Communication model

We consider a mmW single-user multiple-input-multiple-output (MIMO) wireless system with a transmitter (base station, BS) at location[1] $\mathbf{q} \in \mathbb{R}^2$ and a receiver (mobile station, MS) at location $\mathbf{p} \in \mathbb{R}^2$, equipped with an array of N and M antenna elements, respectively. We assume $\mathbf{q}$ known, whereas $\mathbf{p}$ is not. Also, we denote by α the relative 2D-rotation between the transmit and receiving antenna arrays. Figure 1 illustrates the geometry of the aforementioned communication system.

Assuming that the line-of-sight (LOS) link is the dominant path, the input-output relation is

$$y(t) = \sqrt{P_{\text{tx}}} h \mathbf{w}^{\text{H}} \mathbf{a}_M(\theta) \mathbf{a}_N^{\text{H}}(\phi) \mathbf{f} x(t-\tau) + \mathbf{w}^{\text{H}} \mathbf{n}(t), \quad (1)$$

where $\mathbf{f} \in \mathbb{C}^N$ and $\mathbf{w} \in \mathbb{C}^M$ are the transmit and receive unit-norm beamforming vectors, generated from codebooks $\mathcal{F}$ and $\mathcal{W}$ with size N_t^b and N_r^b, respectively; $\mathbf{n}(t)$ is additive white gaussian noise (AWGN) with power spectral density (PSD) N_0, $\tau = \|\mathbf{q} - \mathbf{p}\|/c$ is the time-delay of the LOS path for speed of light c; $x(t)$ and $y(t)$ are the continuous

[1]The extension to 3-dimensions is straightforward. However, it requires the utilization of 2-dimensional antenna arrays.

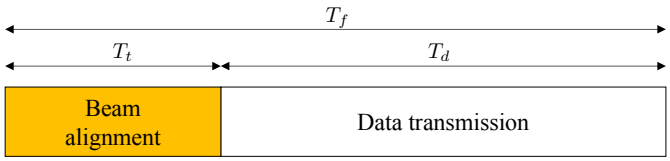

Figure 2. Communication over frames of duration T_f, with data transmission at an effective rate R. More time spent during beam alignment (duration T_f leads to better SNR for data transmission and improved PREB), but a reduction in T_d.

time-domain transmitted and received signals of bandwidth B and duration T_s, with $1/T_s \int_0^{T_s} |x(t)|^2 \mathrm{d}t = 1$; $h \in \mathbb{C}$ is the dominant channel coefficient; P_{tx} is the transmission power; $\mathbf{a}_N(\phi) \in \mathbb{C}^N$ and $\mathbf{a}_M(\theta) \in \mathbb{C}^M$ are the receive and transmit array response vectors for the angle-of-departure (AoD) ϕ and angle-of-arrival (AoA) θ of the dominant path. Note that ϕ and θ are related through $\alpha = \pi - \theta + \phi$. For simplicity of the exposition, but without loss of generality, we will assume that $x(t)$ has flat spectrum, i.e., $X(\omega)$ is constant, with $|X(\omega)|^2 = T_s/(2\pi B)$.

Without loss of generality, we assume a uniform linear array (ULA) with isotropic element gain and $d = \lambda/2$ element separation, where λ is the carrier wavelength. In that case

$$[\mathbf{a}_M(\theta)]_m = e^{j\frac{2\pi d}{\lambda}(m-1)\sin(\theta)}, m \in \{1, \ldots, M\}, \quad (2)$$

with a similar definition for $\mathbf{a}_N(\phi)$.

Communication occurs over frames of fixed duration T_f, of which a time $T_t = nT_s$ with $n \in \mathbb{N}_+$ is devoted to beam alignment (i.e., determining the best $\mathbf{w}$ and $\mathbf{f}$), while the remainder $T_d = T_f - T_t$ is used for data transmission.

B. Performance metrics

We consider two performance metrics: effective data rate R and position-rotation error bound (PREB).

- *Effective data rate R:* Assuming the beams selected for data transmission, after beam alignment are $\mathbf{w}$ and $\mathbf{f}$, then

$$R = \left(1 - \frac{T_t}{T_f}\right) \log_2 \left(1 + \frac{|h|^2 P_{\text{tx}} S(\mathbf{w}, \mathbf{f}, \theta, \phi)}{\sigma^2}\right), \quad (3)$$

  where $S(\mathbf{w}, \mathbf{f}, \theta, \phi) \triangleq |\mathbf{w}^H \mathbf{a}_M(\theta)|^2 |\mathbf{f}^H \mathbf{a}_N(\phi)|^2$, $\sigma^2 = N_0 B$ is the noise power over the signal bandwidth. Note that for a fixed T_t, the rate is maximized when $\mathbf{f} = 1/\sqrt{N}\mathbf{a}_N(\phi)$ and $\mathbf{w} = 1/\sqrt{M}\mathbf{a}_M(\theta)$.
- *PREB:* Assuming a total of $K \leq N_t^b N_r^b$ transmit/receive beam combinations $(\mathbf{f}_k, \mathbf{w}_k)$ are used, we can compute the Fisher Information Matrix (FIM) associated with $[\mathbf{p}, \alpha]$. The PREB is derived from the inverse of this FIM, and provides a lower bound, in the positive semi-definite sense on the achievable estimation accuracy of $[\mathbf{p}, \alpha]$. The mathematical definition of PREB will be provided in Section III-C.

Increasing K will improve the PREB and SNR, but also lead to an increase in T_t, thus leaving less time for data transmission. Hence, there is a natural tension between rate and PREB. Our goal is to understand and quantify this trade-off (see Figure 2).

III. Rate and PREB Computation

A. Codebook and search strategy assumptions

The effective data rate and the PREB depend on the codebook size and the beam alignment strategy. For simplicity, we consider $\mathcal{F}$ and $\mathcal{W}$ to comprise $N_t^b = N$ and $N_r^b = M$ orthogonal vectors, respectively. Specifically, let $\mathbf{f}_i$ and $\mathbf{w}_j$ be the column of a Discrete Fourier Transform (DFT) N-size and M-size matrices, respectively. In addition, we consider an exhaustive search strategy, such that $K = NM$. Other search strategies (e.g., hierarchical search) as well as other codebooks can be analyzed in a similar manner. In addition, we will assume that the MS and BS are able to determine the optimal beams that maximize the SNR. Performing the analysis when this assumption is removed, is a topic of further study.

B. Effective data rate

Under the assumed codebooks and search strategy, the effective data rate is given by

$$R = \left(1 - \frac{NMT_s}{T_f}\right) \log_2 \left(1 + \frac{|h|^2 P_{\text{tx}} \mathrm{S}(\mathbf{w}^*, \mathbf{f}^*, \theta, \phi)}{\sigma^2}\right), \quad (4)$$

in which the optimal beams are those that maximize the SNR:

$$[\mathbf{w}^*, \mathbf{f}^*] = \arg \max_{\substack{\mathbf{w} \in \mathcal{W} \\ \mathbf{f} \in \mathcal{F}}} \frac{|h|^2 P_{\text{tx}} \mathrm{S}(\mathbf{w}, \mathbf{f}, \theta, \phi)}{\sigma^2}. \quad (5)$$

Clearly, if T_f is fixed, then a trade-off between rate and the training overhead exists. More specifically, by increasing the number of antennas, thus the codebook size, the pre-log factor is reduced, thus reducing the time available for data transmission. On the other hand, with more antennas, SNR gains in (5) increase, thus increasing the log factor.

C. PREB from Fisher information

1) PREB definition: Introducing $\boldsymbol{\xi} \triangleq [\mathbf{p}^{\mathrm{T}}, \alpha, h]^{\mathrm{T}}$ with an associated FIM $\mathbf{J}_{\boldsymbol{\xi}}$, obtained from aggregating information during the exhaustive beam alignment strategy, the PREB comprised two components: the position error bound

$$\mathrm{PEB} = \sqrt{\mathrm{trace}\left([\mathbf{J}_{\boldsymbol{\xi}}^{-1}]_{1:2,1:2}\right)}, \quad (6)$$

expressed in meters, and the rotation error bound

$$\mathrm{REB} = \sqrt{[\mathbf{J}_{\boldsymbol{\xi}}^{-1}]_{3,3}}, \quad (7)$$

expressed in radians (or degrees, after conversion). Due to the additive nature of Fisher information,

$$\mathbf{J}_{\boldsymbol{\xi}} = \sum_{\substack{\mathbf{w} \in \mathcal{W} \\ \mathbf{f} \in \mathcal{F}}} \mathbf{J}_{\boldsymbol{\xi}}(\mathbf{f}, \mathbf{w}), \quad (8)$$

where $\mathbf{J}_{\boldsymbol{\xi}}(\mathbf{f}, \mathbf{w})$ is the FIM associated with a single beam pair $(\mathbf{f}, \mathbf{w})$. Hence, we only need to determine an expression for $\mathbf{J}_{\boldsymbol{\xi}}(\mathbf{f}, \mathbf{w})$.

2) FIM for a single beam: Given $(\mathbf{f}, \mathbf{w})$, the FIM $\mathbf{J}_{\boldsymbol{\xi}}(\mathbf{f}, \mathbf{w})$ will be derived, from the observation model (1). We denote the deterministic part of the received signal $y(t)$ by $u(t) \triangleq \sqrt{P_{\text{tx}}}\mathbf{w}^{\text{H}} h \mathbf{a}_M(\theta)\mathbf{a}_N^{\text{H}}(\phi)\mathbf{f}x(t-\tau)$. Also, we express the geometric relationship between the vector $\boldsymbol{\eta} \triangleq [h, \theta, \phi, \tau]^{\tau}$ including the channel parameters with the unknown position $\mathbf{p}$ and rotation α as

$$\begin{bmatrix} p^x \\ p^y \\ \alpha \end{bmatrix} = \begin{bmatrix} q^x + c\tau\cos(\phi) \\ q^y + c\tau\sin(\phi) \\ \pi + \phi - \theta \end{bmatrix}, \tag{9}$$

where q^x q^y are the x and y coordinates of the known transmitter location.

The PREB can be computed from the inverse of the FIM $\mathbf{J}_{\boldsymbol{\xi}}(\mathbf{f}, \mathbf{w})$ given by $\mathbf{J}_{\boldsymbol{\xi}}(\mathbf{f}, \mathbf{w}) = \mathbf{T}\mathbf{J}_{\boldsymbol{\eta}}(\mathbf{f}, \mathbf{w})\mathbf{T}^{\text{T}}$, where

$$\mathbf{T} = \begin{bmatrix} \mathbf{0} & \boldsymbol{\Upsilon} \\ \mathbf{I}_2 & \mathbf{0} \end{bmatrix} \in \mathbb{R}^{5\times 5}, \tag{10}$$

in which $\mathbf{I}_2$ is 2×2 identity matrix, $\boldsymbol{\Upsilon}$ is given by

$$\boldsymbol{\Upsilon} = \frac{1}{c}\begin{bmatrix} -\sin(\phi)/\tau & -\sin(\phi)/\tau & \cos(\phi) \\ \cos(\phi)/\tau & \cos(\phi)/\tau & \sin(\phi) \\ -c & 0 & 0 \end{bmatrix}, \tag{11}$$

and $\mathbf{J}_{\boldsymbol{\eta}}(\mathbf{f}, \mathbf{w}) \in \mathbb{R}^{5\times 5}$ is the FIM for the estimation of the channel parameters $\boldsymbol{\eta}$ from beam pair $(\mathbf{f}, \mathbf{w})$.

The FIM of the channel parameters, associated with a single beam pair can be computed as

$$\mathbf{J}_{\boldsymbol{\eta}}(\mathbf{f}, \mathbf{w}) = \frac{1}{N_0}\int_0^{T_s} \Re\{\nabla_{\boldsymbol{\eta}}^{\text{H}} u(t) \nabla_{\boldsymbol{\eta}} u(t)\}\, \mathrm{d}t. \tag{12}$$

We denote the entries of $\mathbf{J}_{\boldsymbol{\eta}}(\mathbf{f}, \mathbf{w})$ by

$$J_{x,x'} = \frac{1}{N_0}\int_0^{T_s} \Re\left\{\frac{\partial u^*(t)}{\partial x}\frac{\partial u(t)}{\partial x'}\right\}\mathrm{d}t. \tag{13}$$

The entries in the FIM are given by (see Appendix)

$$J_{\tau,\tau} = \frac{P_{\text{tx}}T_s}{N_0}|h|^2|q_f|^2|q_w|^2B^2\pi^2/3, \tag{14}$$

$$J_{\phi,\phi} = \frac{P_{\text{tx}}T_s}{N_0}|h|^2|q_w|^2|\dot{q}_f|^2, \tag{15}$$

$$J_{\phi,h_I} = \frac{P_{\text{tx}}T_s}{N_0}|q_w|^2\Re\left\{h^* q_f^* \dot{q}_f\right\}, \tag{16}$$

$$J_{\phi,h_Q} = \frac{P_{\text{tx}}T_s}{N_0}|q_w|^2\Re\left\{jh^* q_f^* \dot{q}_f\right\}, \tag{17}$$

$$J_{\theta,\theta} = \frac{P_{\text{tx}}T_s}{N_0}|h|^2|q_f|^2|\dot{q}_w|^2, \tag{18}$$

$$J_{\theta,h_I} = \frac{P_{\text{tx}}T_s}{N_0}|q_f|^2\Re\left\{h^* q_w \dot{q}_w^*\right\}, \tag{19}$$

$$J_{\theta,h_Q} = \frac{P_{\text{tx}}T_s}{N_0}|q_f|^2\Re\left\{jh^* q_w \dot{q}_w^*\right\}, \tag{20}$$

$$J_{h,h} = \frac{P_{\text{tx}}T_s}{N_0}\begin{bmatrix} |q_f|^2|q_w|^2 & 0 \\ 0 & |q_f|^2|q_w|^2 \end{bmatrix}, \tag{21}$$

where * indicates the complex conjugate, and we have considered $h = [h_I, h_Q]^{\text{T}}$, $q_w \triangleq \mathbf{w}^{\text{H}}\mathbf{a}_M(\theta)$, $q_f \triangleq \mathbf{f}^{\text{H}}\mathbf{a}_N(\phi)$, $\dot{q}_w = \mathbf{a}_M^{\text{H}}(\theta)\mathbf{D}_r^{\text{H}}\mathbf{w}$ and $\dot{q}_f = \mathbf{a}_N^{\text{H}}(\phi)\mathbf{D}_t^{\text{H}}\mathbf{f}$, in which $\mathbf{D}_t \in \mathbb{C}^{N\times N}$, $\mathbf{D}_r \in \mathbb{C}^{M\times M}$ are diagonal matrices with the k-th entry give by $D_{t,k} = j\pi(k-1)\cos(\phi)$ and $D_{r,k} = j\pi(k-1)\cos(\theta)$, respectively. In addition, $J_{\tau,x} = 0$ for $x \neq \tau$.

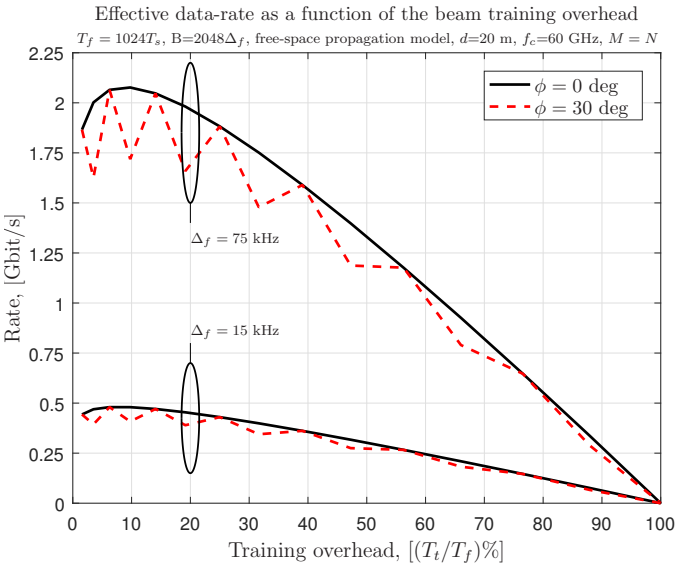

Figure 3. Effective data rate with exhaustive beam training strategy. Black and red lines refers to two different locations of the MS corresponding to d =20 m and $\phi = 0$ and $\phi = 30$ deg.

IV. Simulation Results

In this section, we study the impact of codebook size on the effective data rate and position-rotation bound, as well as the trade-off between these two metrics.

A. Simulation setup

We focus on an idealized MIMO-orthogonal frequency-division multiplexing (OFDM) communication system with 2048 subcarriers, time-frequency efficiency equal to one, inter-carrier spacing $\Delta_f \in \{15 \text{ kHz}, 75 \text{ kHz}\}$, fixed transmission power $P_{\text{tx}} = 27$ dBm, $N = M$, and carrier frequency 60 GHz. One beam during beam alignment corresponds to one OFDM symbol, so $T_s \in \{67\ \mu\text{s}, 13\ \mu\text{s}\}$ and $E_s = P_{\text{tx}}T_s$. Finally, we fix the frame length T_f to 1024 OFDM symbols. This implies that for $N = M = 32$, $T_t/T_f = 1$. We consider the MS location to have a fixed distance of 20 m to the BS and $\alpha = 0$. We study $\phi = 0$ deg and $\phi = 30$ deg, while keeping $\alpha = 0$, allowing us to analyze the effect of beam misalignment.

B. Trade-off between rate and training overhead

Figure 3 shows the effective data rate as a function of the training overhead (T_t/T_f in percentage). We observe that, under our assumptions, there exist an optimum codebook size that maximizes the rate. Namely, for $\phi = 0$, the rate is maximized when $T_t/T_f = 6.25\%$ (corresponding to $N = M = 8$) and 9.76% (corresponding to $N = M = 10$) for $\Delta_f = 15$ kHz and $\Delta_f = 75$ kHz, respectively. Note that the maximum rate

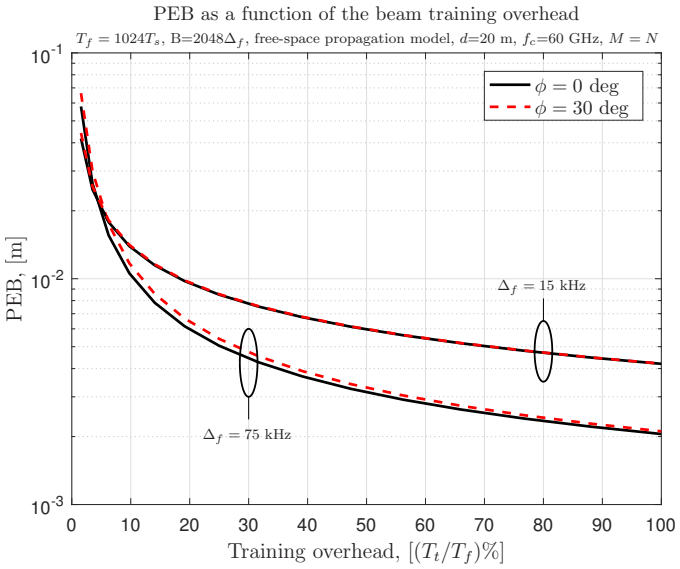

Figure 4. Performance of the PEB as a function of the beam training overhead using sequential search strategy.

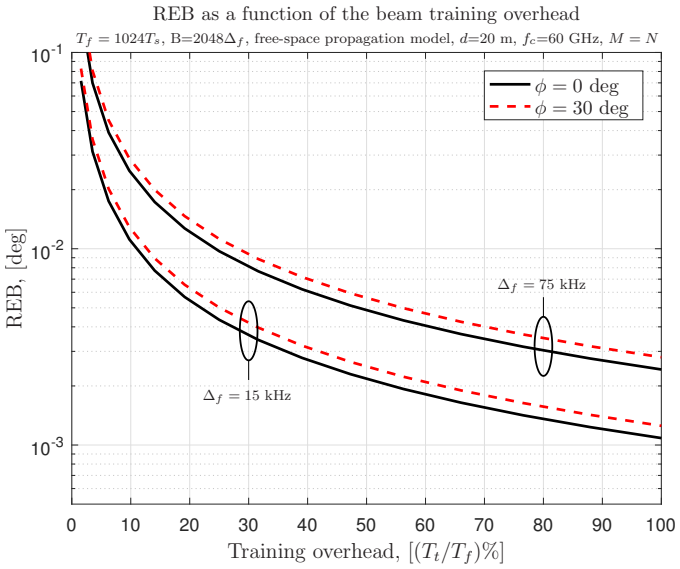

Figure 5. Performance of the REB as a function of the beam training overhead using sequential search strategy.

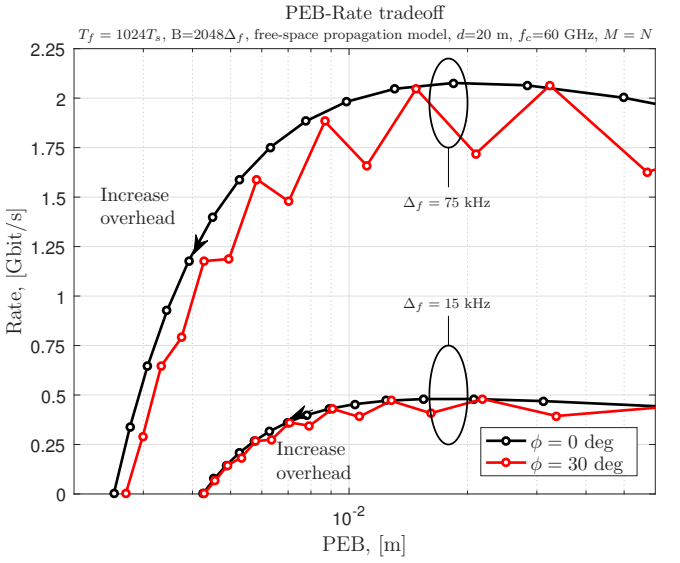

Figure 6. Trade-off between the PEB and the effective rate when varying the training overhead. Arrows indicate increase in $N = M$.

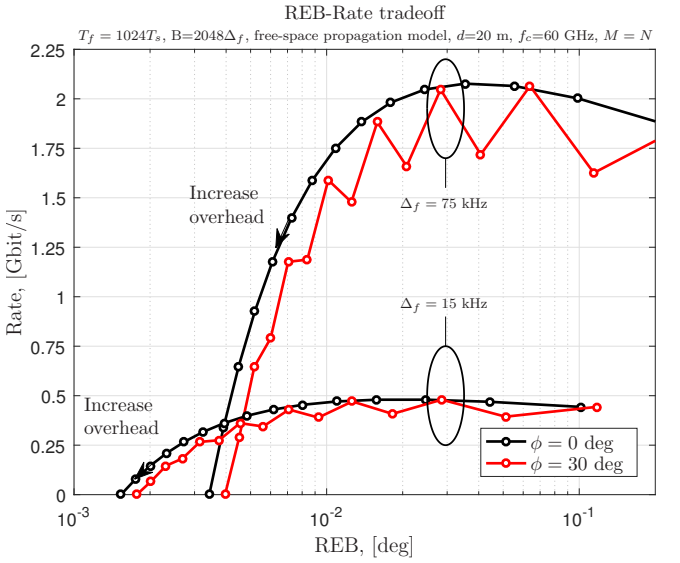

Figure 7. Trade-off between the REB and the effective rate when varying the training overhead. Arrows indicate increase in $N = M$.

does not scale linearly with the bandwidth, due to the slight increase in training overhead. For $\phi \neq 0$, beam misalignment due to relative location and orientation of the transmitter and receiver has a (limited) impact on the rate, which is more pronounced for larger Δ_f.

C. Trade-off between PREB and training overhead

Figures 4 and 5 show the position error bound (PEB) and rotation error bound (REB), respectively, as a function of the training overhead. In contrast to the rate, we note that both improve with increased training, as more Fisher information is collected (see (12)). We again notice a dependence on ϕ, where the misalignment leads to small increase in both PEB and REB. Interestingly, the signal bandwidth affects PEB and REB in a different way: while the PEB benefits from a large bandwidth, because of a more accurate ranging, the REB, which depends only on the bearing estimation, is more precise with signal with smaller bandwidth as the energy E_s is higher.

D. Positioning and data-rate trade-off

While the above results in terms of rate and PREB are largely well-established, our model allows to study their trade-off. Figures 6 and 7 depict the trade-off between the effective data rate and positioning metrics (PEB and REB). More specifically, the trade-off curves are obtained by varying the training overhead (thus beamwidth) from 1.5% to 100%, corresponding to $N = M = 4$ and $N = M = 32$, respectively. As before, we consider the cases of $\Delta_f = 15$kHz, $\Delta_f = 75$kHz, $\phi = 0$ deg and $\phi = 30$ deg.

For the PEB (Figure 6), the location accuracy achieved at the maximum data rate ($\approx$ 10% training overhead) is approximately 1 cm, irrespective of the bandwidth. This is comparable to the state-of-the-art RTK GPS, but relies only on the mmW radio signal from a single base station. We conclude that increasing the signal bandwidth improves *both* the rate and the PEB. Thus, these two performance metrics are not in conflict.

In terms of REB (Figure 7), for the maximum data rate, the REB is around 0.03 degrees. In contrast to the PEB, the plots related to the trade-off between rate and REB show that by varying the bandwidth, there is a point in which the effective rate vs REB curves intersect. This point corresponds to an overhead of 87% with $\Delta_f = 75$kHz and 39% with $\Delta_f = 15$kHz. In other words, it is possible to reach the same rate and REB by either designing a system with low bandwidth and low overhead or with higher bandwidth and higher overhead.

V. Conclusion

In this paper we considered a mmW communication system and studied the feasibility of utilizing the beam training period for positioning. We investigated the trade-off between positioning and data rate in LOS channel conditions. The following conclusions were drawn: (i) a high training overhead can cancel out the gain from highly directional beamforming; (ii) accurate position and rotation estimation can be achieved using the training signal used for beam alignment; (iii) given a fixed transmit power, a small signal bandwidth is desirable for rotation estimation; and (iv) the PEB and REB associated with the maximum effective rate is largely independent of the bandwidth. Extensions of the work include the multi-user case, different types of codebooks, the impact of array calibration errors, and the removal of the optimal beam assumption.

Appendix

Here we derive the expressions for the entries of the FIM. First, we note that the derivative terms are given by

$$\frac{\partial}{\partial \tau}u(t) = -hq_w q_f^* \dot{x}(t-\tau), \tag{22}$$

$$\frac{\partial}{\partial \phi}u(t) = hq_w \dot{q}_f^* x(t-\tau), \tag{23}$$

$$\frac{\partial}{\partial \theta}u(t) = h\dot{q}_w q_f^* x(t-\tau), \tag{24}$$

$$\frac{\partial}{\partial h_I}u(t) = q_w q_f^* x(t-\tau), \tag{25}$$

$$\frac{\partial}{\partial h_Q}u(t) = jq_w q_f^* x(t-\tau), \tag{26}$$

where $\dot{x}(t-\tau) = \partial x(t-\tau)/\partial\tau$ and $\dot{q}_f, \dot{q}_w$ were defined in Section III-C.

Then, substitution into (13) leads to

$$J_{\tau,\tau} = \frac{P_{\text{tx}}}{N_0}\int_0^{T_s} \Re\left\{h^* h q_w^* q_w q_f^* q_f \dot{x}^*(t-\tau)\dot{x}(t-\tau)\right\}\mathrm{d}t \tag{27}$$

$$= \frac{P_{\text{tx}}}{N_0}|h|^2|q_f|^2|q_w|^2\int_{-\pi B}^{\pi B}|j\omega X(\omega)|^2\,\mathrm{d}\omega$$

$$= \frac{E_s}{N_0}\frac{B^2\pi^2}{3}|h|^2|q_f|^2|q_w|^2,$$

where we used the Parseval's identify to change to frequency domain and us the fact that $|X(\omega)|^2 = T_s/(2\pi B)$. Since $X(\omega)$ is symmetric, we find that $J_{\tau,\phi} = J_{\tau,\theta} = J_{\tau,h_I} = J_{\tau,h_Q} = 0$.

The remaining terms are given by

$$J_{\phi,\phi} = \frac{P_{\text{tx}}}{N_0}\int_0^{T_s} \Re\left\{h^* h q_w^* q_w \dot{q}_f \dot{q}_f^* x^*(t-\tau)x(t-\tau)\right\}\mathrm{d}t \tag{28}$$

$$= \frac{P_{\text{tx}}}{N_0}|h|^2|q_w|^2|\dot{q}_f|^2\int_{-\pi B}^{\pi B}|X(\omega)|^2\,\mathrm{d}\omega = \frac{E_s}{N_0}|h|^2|q_w|^2|\dot{q}_f|^2,$$

since $\int_{-\pi B}^{\pi B}|X(\omega)|^2 = 1$ by assumption. Similarly,

$$J_{\phi,\theta} = \frac{P_{\text{tx}}}{N_0}\int_0^{T_s} \Re\left\{h^* h q_w^* \dot{q}_w q_f^* \dot{q}_f x^*(t-\tau)x(t-\tau)\right\}\mathrm{d}t \tag{29}$$

$$= \frac{E_s}{N_0}|h|^2\Re\{q_f^* q_w^* \dot{q}_f \dot{q}_w\},$$

$$J_{\phi,h_I} = \frac{P_{\text{tx}}}{N_0}\int_0^{T_s} \Re\left\{h^* q_w^* q_w q_f^* \dot{q}_f x(t-\tau)x^*(t-\tau)\right\}\mathrm{d}t \tag{30}$$

$$= \frac{E_s}{N_0}|q_w|^2\Re\left\{h^* q_f^* \dot{q}_f\right\},$$

$$J_{\phi,h_Q} = \frac{P_{\text{tx}}}{N_0}\int_0^{T_s} \Re\left\{jh^* q_w^* q_w q_f^* \dot{q}_f x(t-\tau)x^*(t-\tau)\right\}\mathrm{d}t \tag{31}$$

$$= \frac{E_s}{N_0}|q_w|^2\Re\left\{jh^* q_f^* \dot{q}_f\right\},$$

$$J_{\theta,\theta} = \frac{P_{\text{tx}}}{N_0}\int_0^{T_s} \Re\left\{h^* h q_f^* q_f \dot{q}_w^* \dot{q}_w x^*(t-\tau)x(t-\tau)\right\}\mathrm{d}t \tag{32}$$

$$= \frac{E_s}{N_0}|h|^2|q_f|^2|\dot{q}_w|^2,$$

$$J_{\theta,h_I} = \frac{P_{\text{tx}}}{N_0}\int_0^{T_s} \Re\left\{h^* \dot{q}_w^* q_w q_f q_f^* x(t-\tau)x^*(t-\tau)\right\}\mathrm{d}t \tag{33}$$

$$= \frac{E_s}{N_0}|q_f|^2\Re\left\{h^* q_w \dot{q}_w^*\right\},$$

$$J_{\theta,h_Q} = \frac{P_{\text{tx}}}{N_0}\int_0^{T_s} \Re\left\{jh^* \dot{q}_w^* q_w q_f q_f^* x(t-\tau)x^*(t-\tau)\right\}\mathrm{d}t \tag{34}$$

$$= \frac{E_s}{N_0}|q_f|^2\Re\left\{jh^* q_w \dot{q}_w^*\right\},$$

$$J_{h_I,h_I} = \frac{P_{\text{tx}}}{N_0}\int_0^{T_s} \Re\left\{q_w^* q_w q_f^* q_f x(t-\tau)x^*(t-\tau)\right\}\mathrm{d}t \quad (35)$$
$$= \frac{E_s}{N_0}|q_f|^2|q_w|^2,$$

$$J_{h_I,h_Q} = \frac{P_{\text{tx}}}{N_0}\int_0^{T_s} \Re\left\{j q_w^* q_w q_f^* q_f x(t-\tau)x^*(t-\tau)\right\}\mathrm{d}t = 0, \quad (36)$$

$$J_{h_Q,h_Q} = \frac{P_{\text{tx}}}{N_0}\int_0^{T_s} \Re\left\{q_w^* q_w q_f^* q_f x(t-\tau)x^*(t-\tau)\right\}\mathrm{d}t \quad (37)$$
$$= \frac{E_s}{N_0}|q_f|^2|q_w|^2.$$

ACKNOWLEDGMENTS

This work was supported by the EU-H2020 project HIGHTS (High Precision Positioning for Cooperative ITS Applications), Grant No. MG-3.5a-2014-636537; the VINNOVA COPPLAR project, funded under Strategic Vehicle Research and Innovation Grant No. 2015-04849; and the 5Gto10G project funded by Nokia Solutions and Networks Oy, Huawei Technologies Oy (Finland) Co. Ltd, Keysight Technologies Finland Oy and the Finnish Funding Agency for Technology and Innovation (Tekes).

REFERENCES

[1] M. K. Samimi and T. S. Rappaport, "3-D millimeter-wave statistical channel model for 5G wireless system design," *IEEE Transactions on Microwave Theory and Techniques*, vol. 64, no. 7, pp. 2207–2225, 2016.

[2] S. Kutty and D. Sen, "Beamforming for millimeter wave communications: An inclusive survey," *IEEE Communications Surveys Tutorials*, vol. 18, no. 2, pp. 949–973, Secondquarter 2016.

[3] W.-X. Zou, G.-L. Du, B. Li, and Z. Zhou, "Step-wisely refinement based beam searching scheme for 60 ghz communications," *Wirel. Pers. Commun.*, vol. 71, no. 4, pp. 2993–3010, Aug. 2013. [Online]. Available: http://dx.doi.org/10.1007/s11277-012-0985-8

[4] A. Dammann, R. Raulefs, and S. Zhang, "On prospects of positioning in 5G," in *IEEE International Conference on Communication Workshop (ICCW)*, June 2015, pp. 1207–1213.

[5] F. Lemic, J. Martin, C. Yarp, D. Chan, V. Handziski, R. Brodersen, G. Fettweis, A. Wolisz, and J. Wawrzynek, "Localization as a feature of mmWave communication," in *International Wireless Communications and Mobile Computing Conference (IWCMC)*, Sept 2016, pp. 1033–1038.

[6] A. Shahmansoori, G. Garcia, G. Destino, G. Seco-Granados, and H. Wymeersch, "5G position and orientation estimation through millimeter wave MIMO," in *IEEE Global Telecommunications (GLOBECOM) Conference Workshops*, 2015.

[7] S. Jeong, O. Simeone, A. Haimovich, and J. Kang, "Beamforming design for joint localization and data transmission in distributed antenna system," *IEEE Transactions on Vehicular Technology*, vol. 64, no. 1, pp. 62–76, 2015.

[8] N. Garcia, H. Wymeersch, E. G. Ström, and D. Slock, "Location-aided mm-wave channel estimation for vehicular communication," in *IEEE 17th International Workshop on Signal Processing Advances in Wireless Communications (SPAWC)*, July 2016, pp. 1–5.

[9] J. C. Aviles and A. Kouki, "Position-aided mm-wave beam training under nlos conditions," *IEEE Access*, vol. 4, pp. 8703–8714, 2016.